Active Control of Laser Wavefronts in Atom Interferometers

A. Trimeche, M. Langlois, S. Merlet, and F. Pereira Dos Santos*

LNE-SYRTE, Observatoire de Paris, PSL Research University, CNRS, Sorbonne Universités, UPMC Univ. Paris 06, 61 Avenue de l'Observatoire, 75014 Paris, France

(Received 16 August 2016; revised manuscript received 9 December 2016; published 23 March 2017)

Wavefront aberrations are identified as a major limitation in quantum sensors. They are today the main contribution in the uncertainty budget of the best cold-atom interferometers based on two-photon laser beam splitters and constitute an important limit for their long-term stability, impeding these instruments from reaching their full potential. Moreover, they will also remain a major obstacle in future experiments based on large-momentum beam splitters. In this article, we tackle this issue by using a deformable mirror to control actively the laser wavefronts in atom interferometry. In particular, we demonstrate in an experimental proof of principle the efficient correction of wavefront aberrations in an atomic gravimeter.

DOI: 10.1103/PhysRevApplied.7.034016

I. INTRODUCTION

Inertial sensors based on atom interferometry [1], such as gravimeters and gradiometers [2–6] or gyroscopes [7,8], are subject today to intense developments, owing to their large range of applications, in geophysics, navigation, space science, and high-precision measurements in fundamental physics [9–11]. In light-pulse atom interferometers [12], the final phase shift depends on the acceleration and the rotation of the experimental setup with respect to the inertial reference frame defined by the atoms in free fall. The inertial force is then derived from the measurement of the relative displacement of these atoms compared to the lasers' equiphases. Distortions of these equiphases thus induce parasitic phase shifts which bias the measurement. This effect is linked to the residual ballistic motion of the atoms in the laser beam profile during their free fall as displayed on the left in Fig. 1. Wavefront aberrations are identified and measured on atom interferometers [13–15] as the major source of bias uncertainty and long-term instability in the best light-pulse atom interferometers used as inertial sensors, such as high-precision gravimeters [3,4] and gyroscopes [8,16,17]. This is also true for next-generation experiments, such as those based on large-momentum beam splitters [18], as well as in future space projects [19].

The influence of wavefront aberrations can, in principle, be limited, if not suppressed, by performing atom interferometry inside a cavity, such as in Ref. [20], which allows for spatial mode selection and filtering. Yet, the requirement of operating the interferometer with large laser waists, of the order of a centimeter radius size, in a compact cavity puts severe constraints on the realization and alignment for stable operation and for avoiding the coupling of unwanted transverse modes, which otherwise induce large wavefront aberrations [21].

In astronomy, wavefront distortions and their fluctuations due to atmospheric turbulence also impose severe limits to the resolution of large-area telescopes. To overcome this problem, deformable mirrors (DMs) have been proposed [22] and developed [23] for the efficient real-time correction of wavefront aberrations. They are based on different technologies such as the nine-actuator deformable electrostatic membrane using continuous voltage distribution [24], 35-actuator bimorph deformable mirror composed of two disks of lead magnesium niobate [25], and thin polymer membrane with permanent magnets and microcoils [26]. DMs are already used to correct wavefront aberrations of laser beams, potentially in a closed loop [27], and, for instance, with a thermally deformable mirror [28], in various fields such as ophthalmology, optical beam interferometry, and femtosecond pulse shaping. DMs can also be used for tailoring the shape of the cavity eigenmodes [29] and, thus, selecting the coupled transverse modes. Last, it enables one to generate flat-top laser beams [30], which are of interest for light pulse atom interferometry.

Here, a DM is used to control the laser wavefront in an atom interferometer. We demonstrate its ability and efficiency to correct the wavefront aberrations in a proof-of-principle experiment realized with an atomic gravimeter.

II. DESCRIPTION OF THE EXPERIMENT

The sensor head of the gravimeter is described in Ref. [31]. The laser system, which is realized using two extended cavity laser diodes, and a typical measurement sequence are detailed in Ref. [32]. In this compact experimental setup, atoms are loaded directly from a background ^{87}Rb vapor, trapped in a three-dimensional magneto-optical trap (MOT), and further cooled down to 2 μK before being dropped in free fall by switching off the

*franck.pereira@obspm.fr

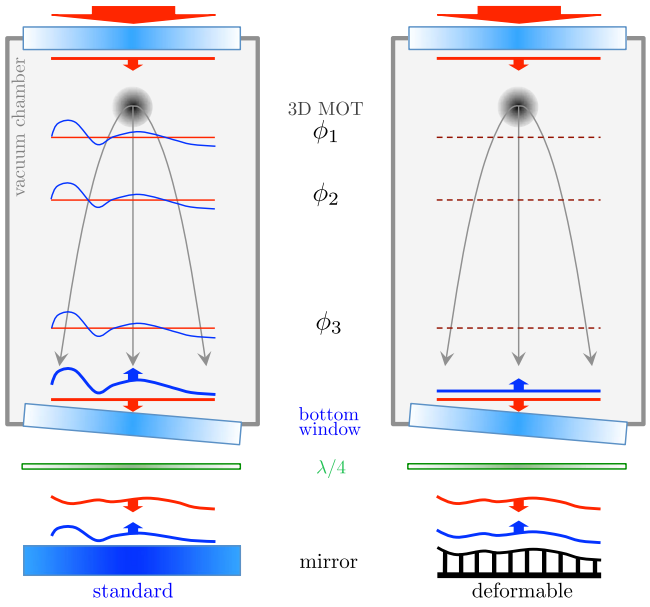

FIG. 1. Laser wavefronts propagation. The laser beam enters the vacuum chamber from the top and exits through the bottom window. The descending wavefront is taken as flat (red line). After being reflected by a standard mirror (left) or a deformable mirror (right), it reenters the vacuum chamber (blue line). Left: The ascending wavefront gets distorted by the aberrations of the bottom window, $\lambda/4$ plate, and standard mirror. The laser phase difference then depends on the transverse position. It gets sampled differently at the three pulses depending on the ballistic trajectories of the atoms, which leads to a bias. Right: The ascending wavefront is corrected by properly shaping the deformable mirror. This leads to uniform laser phase differences and no bias.

cooling lasers. The interferometer is obtained by pulsing counterpropagating laser beams in the vertical direction. Two copropagating vertical laser beams, of wave vectors $\vec{k}_1$ and $\vec{k}_2$, are first overlapped and delivered to the atoms through a single collimator. The counterpropagating beams are obtained by a reflection on a mirror. Because of the Doppler shift induced by the free fall of the atoms, only two counterpropagating beams will drive the stimulated Raman transitions according to the two-photon resonance condition. A three-Raman-pulse sequence $\frac{\pi}{2} - \pi - \frac{\pi}{2}$ allows one to split, deflect, and recombine the atomic wave packets, thus realizing a Mach-Zehnder–type interferometer. With this geometry, the atomic phase shift at the output of the interferometer is given by [33] $\Delta\Phi = \phi_1 - 2\phi_2 + \phi_3$, where ϕ_i is the phase difference between the two Raman lasers, at the position $\vec{z}_i$ of the center of mass of the wave packet, at the time of the ith Raman pulse. For an ideal plane wavefront, $\phi_i^p = \vec{k}_{\text{eff}}\vec{z}_i$, which leads to $\Delta\Phi^p = -\vec{k}_{\text{eff}}\vec{g}T^2$, where $\vec{k}_{\text{eff}} = \vec{k}_1 - \vec{k}_2$ is the effective wave vector, $\vec{g}$ the acceleration of Earth's gravity, and T the free-evolution time between two consecutive Raman pulses. Such atomic accelerometers are thus sensitive to the relative acceleration between the free-falling atoms and the retroreflecting mirror, which sets the phase reference for the Raman lasers. Any deviation of the phase regarding to ϕ_i^p might lead to a bias on the gravity measurement due to the expansion of the atomic cloud across the lasers wavefronts (see Fig. 1).

III. CHARACTERIZATION OF THE MIRROR

In our setup, the retroreflecting mirror (and an additional quarter-wave plate) are placed outside the vacuum chamber as shown in Fig. 1. Formerly, as described in Ref. [32], we have used a standard dielectric mirror and obtained at best a sensitivity of 60 μGal in 1 s measurement time (1 $\mu\text{Gal} = 10^{-8}$ ms^{-2}). For this study, the mirror is replaced by a Kilo-C-DM MEMS deformable mirror from Boston Micromachines Corporation with a 9.9-mm diameter of the active circular surface. This DM uses 952 microactuators, with a pitch of 300 μm, and a maximum stroke of 1.8 μm for an applied voltage of 195 V. The DM surface is a continuous gold-coated membrane, with a specified flatness of 11 nm rms. A homemade software program allows us to control the DM surface shape, by varying the amplitude of the first 64 Zernike polynomials [34], which are conventionally used as a basis to decompose wavefront aberrations. The default setting of the DM is the flat map (FM) configuration, which is calibrated by the constructor in order to make the mirror plane, with optimized voltages for each actuator (around 80 V). This calibration is performed so as to minimize the rms error, and the corresponding measurement performed with a wavefront sensor is provided. From this measurement, we calculate a flatness of 6.47 nm of rms (10.81 nm rms considering the DM rectangular edge) and 28.02 nm of the peak to valley dominated by a residual curvature. This is comparable to the flatness of the best high-quality commercially available dielectric mirrors.

To characterize the response of the DM with respect to the applied voltage, we measure the wavefront deformation of a laser beam reflected by the DM using a Shack-Hartmann (SH) sensor [35] (a HASO model, marketed by the company Imagine Optic). We deform the mirror by applying on each actuator i a voltage $V(i) = V_{\text{FM}}(i) + U.Z(i)$, where $V_{\text{FM}}(i)$ is the setting of the FM configuration, $Z(i)$ is a given Zernike polynomial evaluated at the pixel i, and U is the corresponding amplitude. We then perform differential measurements, subtracting from the deformed wavefront signal the reference FM wavefront. The measurement is performed on several aberrations, corresponding to the lowest-order Zernike polynomials, which are expected to be dominant in our experiment. To illustrate these measurements, we display in Fig. 2 the response of the DM to the amplitude U of the applied voltage for a coma 90° deformation [Fig. 2(a)] and for an astigmatism 0° deformation [Fig. 2(b)]. For weak amplitudes U (below about 20 V),

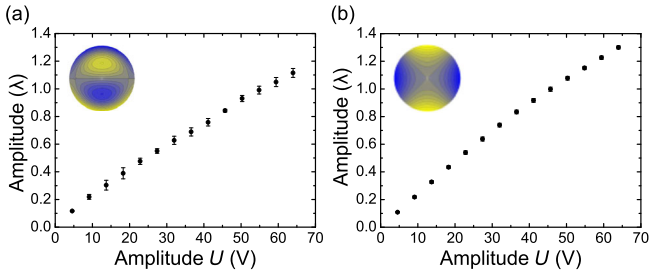

FIG. 2. Amplitude of the DM deformation as a function of the amplitude U of the applied voltage for (a) a coma 90° deformation and (b) an astigmatism 0° deformation.

we find a linear behavior of the actuator motion. Nonlinearities at higher amplitudes make the DM response decrease. We measure an amplitude of $0.025(1)\lambda$ per volt added to the FM voltages, which is twice the surface deformations because of the reflection onto the DM. This is in perfect agreement with the constructor calibrations. In addition, we find the standard deviation of measurements repeated over several days to be lower than $\lambda/125$, limited by the SH repeatability, confirming the DM long-term stability in an open loop [36].

The parasitic phase shifts induced by the wavefront aberrations of the laser beams result from the convolution between the distribution of atomic trajectories and the Raman beam wavefronts and, consequently, depend on many experimental parameters such as the temperature, the initial position and velocity distribution of the atomic cloud, the shape of the Raman beams, etc. Table I lists the expected phase shifts at the output of the interferometer, induced by the most common aberrations, which correspond to some of the first Zernike polynomials. These phase-shift formulas are derived for Raman beams with an infinite size and homogeneous intensity profile and for a point source atomic cloud in a ballistic expansion.

The focus gives an interferometer phase shift independent of the initial positions of the atoms. On the contrary, the shifts due to comas depend linearly on the initial positions. It is thus, in principle, zero when the atomic distribution is centered on the mirror. We actually use this linear dependence to center the atomic cloud on the mirror or/and the mirror on the atomic cloud (see below). As for the astigmatism, it is zero and thus independent of the initial positions of the atoms. However, this is related to averaging the effects of opposite curvatures along orthogonal directions and assumes a radial isotropy. This no longer holds if the velocity distribution (of the detected atoms) is not isotropic, which can be induced by spatial inhomogeneities of the detection. For instance, with Gaussian velocity distributions, eventually different along two orthogonal directions, we obtain $\Delta\Phi = 2k_{\text{eff}}T^2(\sigma_{v_x}^2 - \sigma_{v_y}^2)/R^2$, where $\sigma_{v_{x,y}}$ are the projection of the initial velocity dispersion of the atomic cloud.

Remarkably, most of the first modes of Table I depend on $T^2\sigma_v^2$, where σ_v is the initial velocity dispersion of the atomic ensemble. The corresponding biases on the value of g are therefore independent of T and proportional to the temperature. In contrast, higher-order terms, e.g., spherical aberrations, give biases on g which depend not only on the temperature but also on the value of T.

TABLE I. Interferometer phase shifts due to different aberration orders of the retroreflecting mirror. The phase shifts are averaged over the velocity distribution for initial positions x_0 and y_0 of the atomic cloud. $f(R,x_0,y_0,t_1,T,\sigma_v) = 4[x_0^2 + y_0^2 + \sigma_v^2(6t_1^2 + 12t_1T + 7T^2)] - R^2$, where R is the mirror radius, t_1 is the delay of the first Raman pulse with respect to the release time of the atoms, and σ_v is the initial velocity dispersion of the atomic cloud.

Zernike polynomial (Z_n^m)	$\Delta\Phi$
Piston (Z_0^0), tilts ($Z_1^{\pm1}$)	0
Focus (Z_2^0)	$8k_{\text{eff}}T^2\sigma_v^2/R^2$
Astigmatisms ($Z_2^{\pm2}$)	0
Comas 0° (Z_3^{-1})	$24k_{\text{eff}}T^2x_0\sigma_v^2/R^3$
Coma 90° (Z_3^1)	$24k_{\text{eff}}T^2y_0\sigma_v^2/R^3$
Spherical ab. (Z_4^0)	$24k_{\text{eff}}T^2\sigma_v^2 f(R,x_0,y_0,t_1,T,\sigma_v)/R^4$

IV. MEASUREMENTS WITH AN ATOM INTERFEROMETER

A good control of the mirror and atom parameters (such as centering and alignments) is necessary to characterize the DM impact on the interferometer and compare experimental results with a model of the experiment. For that purpose, a first coarse adjustment of the mirror position is initially performed by maximizing the number of detected atoms. Because of mechanical tolerance and alignment errors, the atomic cloud is not necessarily perfectly aligned with the Raman beams and the center of the detection area. Thanks to additional bias coils, the initial position of the cloud is set so as to maximize the contrast of the interferometer, which corresponds to placing the atomic cloud at the center of the Raman beams. Once the atomic cloud position is fixed, we take advantage of the property of the coma aberration to make a finer adjustment of the DM onto the center of the atomic cloud. Significant coma aberrations are applied on the DM, and the differential bias on g is measured as a function of the mirror position, with respect to the FM configuration, as shown in Fig. 3. As expected, linear dependencies are observed through the east-west (EW) and north-south (NS) directions, which are aligned with the proper axes of the DM. The zero crossing positions (marked by the blue arrows) correspond to the best DM alignment with the center of the atomic cloud.

In order to determine the relationship between the wavefront and the interferometric phase shift, a simulation of an interferometer using a DM has been developed. This Monte Carlo simulation reproduces the experiment

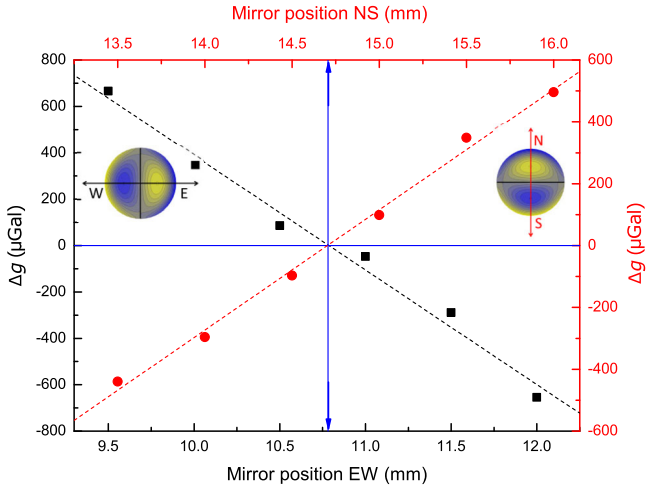

FIG. 3. Effect of comas, of 0.4λ amplitude, on the gravity measurement. The deformable mirror is displaced on the east-west (respectively, north-south) direction with a coma 0° deformation (black squares) [respectively, coma 90° (red circles)].

described in Fig. 1, taking into account the parameters of the atomic source, the inhomogeneity of the detection response (as in Ref. [37]), and the wavefront aberrations. To characterize the DM, the biases of different aberrations on g are measured by varying the mirror shape for $T = 58$ ms. For these measurements, the short-term sensitivity is in the range 100–200 μGal at 1 s. A summary of the comparison between the numerical simulations and the experimental results is shown in Table II. The bias of the focus and the spherical aberration on g are measured for weak deformations of the DM. We find a good agreement for the spherical aberration but a significant difference for the focus, which is not explained. To evaluate the effect of the comas, we set a fixed deformation of 0.4λ and displace the DM on the EW (for the coma 0°) and NS (for the coma 90°) directions, for a fixed position of the cloud (Fig. 3). Here also, experiments are in good agreement with the simulations.

Given the measurement of the DM flatness in the FM configuration, we now evaluate the corresponding bias on the gravity measurement. For that, we consider only the contributions having revolution symmetry such as the focus and the different orders of spherical aberrations. By weighting these contributions with their corresponding measured sensitivities, we estimate a relatively large bias on the gravity measurement of the order of 30 μGal. This

TABLE II. Comparison between simulations and measurements of different aberration biases on g.

Aberration	Measurement	Simulation
Focus	2991(55) μGal/μm	3652(10) μGal/μm
Spherical ab.	3172(110) μGal/μm	3275(10) μGal/μm
Coma 0°/EW	−494(30) μGal/mm	−523(1) μGal/mm
Coma 90°/NS	−503(14) μGal/mm	−522(1) μGal/mm

FM calibration is performed by the manufacturer by minimizing the global rms error, which is not best suited for our application, for which one would minimize aberrations of revolution symmetry (such as the focus, the spherical aberrations, etc.) and would tolerate higher residuals on the other aberrations (tilts, astigmatisms, comas, trefoils, etc.). Given the excellent resolution on the actuator displacement (of the order of 50 pm, in principle), lower biases could be obtained by adjusting the mirror with these constraints, which would improve the accuracy of the gravimeter. Alternatively, comas could be minimized in order to reduce the sensitivity to the initial position of the atomic cloud (see Table I and the measurements below), which would improve the long-term stability of the measurement.

We then evaluate the stability of the gravity measurements when deliberately applying selected aberrations using the DM. First, a differential measurement with two different amplitude of focus (0.1λ and 0.6λ) is performed over 2 days. Figure 4(a) displays the results of this measurement, where each point is averaged over 4400 s (73 min). The observed fluctuations around the average value of 792 μGal are consistent with a white noise, as the corresponding Allan standard deviation is found to decrease as $1/\sqrt{\tau}$ with the averaging time τ. We reach a stability of 4 μGal after 10 h, which corresponds to a remarkable relative stability of 0.5%. This confirms the high stability of the DM in an open loop. Then, we perform differential gravity measurements of a fixed coma 90° with 0.1λ amplitude versus the FM configuration. We observe relatively large and well-resolved variations, displayed in Fig. 4(b), of the order of ± 30 μGal over a day, which we attribute to slow fluctuations of the atomic source initial position (of the order of ± 200 μm) [37]. These position fluctuations bias the gravity measurement in the presence of asymmetric wavefront distortions such as coma aberrations.

V. COMPENSATION OF WAVEFRONT ABERRATIONS

Because of its high stability, the deformable mirror could, in principle, be used to correct the biases caused by the bottom window of the vacuum chamber and the

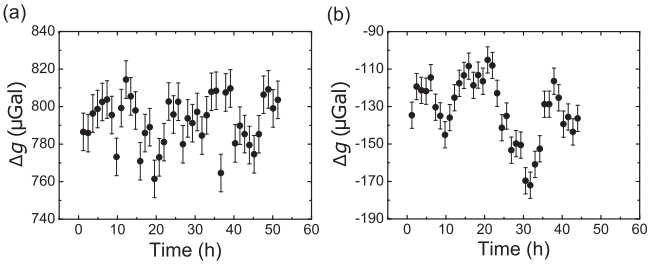

FIG. 4. Differential gravity between (a) two different focus deformations of 0.1λ and 0.6λ amplitudes and (b) a coma 90° deformation with 0.1λ amplitude and the FM configuration.

quarter-wave plate as described in Fig. 1 (right). However, the optical flatness of the view port was not measured before being installed. Furthermore, it is very likely that its properties have been modified by its installation in the experimental chamber, due to mechanical and thermal stresses during the pumping process.

As mentioned before, the wavefront aberration effect on the gravity signal depends on many experimental parameters, which allows one to get some insight on their shape and amplitude. For instance, the size of the atomic detection [14] or the aperture of the Raman beams [15] acts as a filter for the atomic trajectories which contribute to the interferometer signal. Also, the effect of wavefront distortions gets modified when varying the temperature or modifying the initial position of the cloud (see Table I). Remarkably, increasing the initial size of the atomic cloud reduces the contribution of high-frequency components of the wavefront [13]. Measurements of the interferometer phase versus the above-mentioned parameters can be compared with phase shifts calculated for different models of these aberrations [13–15]. But, in the absence of an *a priori* knowledge of the wavefront, the deconvolution from the interferometer response and the averaging over the trajectories is a difficult task, due to nonunicity of the solution of the inverse problem [13]. As a way to overcome this, spatially resolved detection, such as the point source interferometry imaging technique demonstrated in Ref. [38], allows for the measurement of the phase shift as a function of the transverse position in the interferometer laser beam, which is then related only to the initial transverse velocity. This renders the deconvolution simpler and offers the possibility of more accurately reconstructing the wavefront and, thus, retrieving the resulting wavefront aberrations. In that case, one would be able to compensate for these distortions by using a DM. Unfortunately our sensor geometry is not well adapted for the implementation of this technique, due to a lack of optical access.

Instead, and for a proof of principle, a well-characterized optical element is inserted between the bottom window and the mirror, and its effect on the interferometric measurement is compensated by adapting the shape of the mirror. More precisely, we use an additional window of low optical quality, selecting a 9-mm diameter area which presents strong aberrations in order to generate a large bias on the measurements. The wavefront aberrations of this area are initially characterized using the SH, in direct transmission. Figure 5 shows these aberrations, which were decomposed on the Zernike polynomial basis. Dominant contributions are 780(22) nm of astigmatism 0°, −480(15) nm of focus, −370(12) nm of coma 0°, and −60(6) nm of spherical aberration. In order to compensate for the wavefront distortion caused by the additional window, the DM is shaped following the same aberration by summing the above contributions with their respective amplitudes. To assess the efficiency of the wavefront correction by the

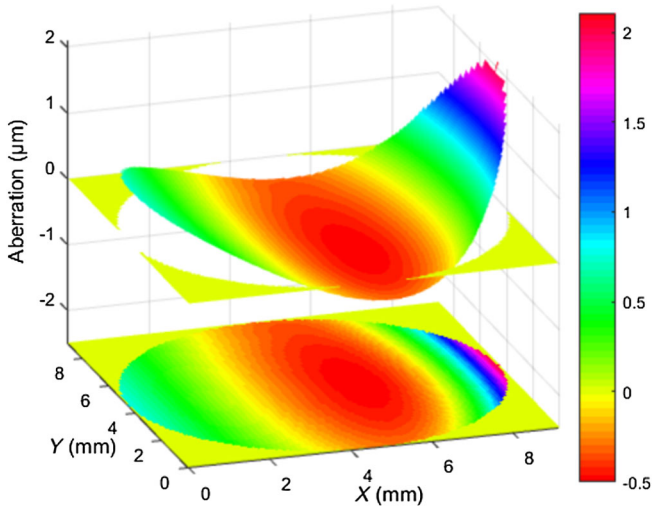

FIG. 5. Aberrations of the additional window measured by a Shack-Hartmann sensor in direct transmission through a 9-mm aperture diaphragm area.

DM, a set of gravity measurements is realized before and after the installation of the additional window for several interferometer times $2T$. Each gravity value is obtained by averaging the results of two measurements performed with two opposite wave-vector directions in order to reject most of the systematic effects [13]. The gravity measurements reported below are differential, taking the value of g measured for $T = 50$ ms with the DM in the FM configuration as a reference. For the reference measurements, the contrast of the interferometer is 17%. The measurement process is done in four steps, and the results are displayed in Fig. 6.

First, a series of reference measurements (represented by open squares) are realized with the DM in the FM configuration before adding the window. Note that, in all the differential measurements, the systematic effect due to the two-photon light shift [39] is not corrected for, which explains most of the observed variation of the measured values of g as a function of T. Second, we add the window, we observe a reduction of the contrast down to 10%, and we measure a change of the gravity value as large as $-1040(10)$ μGal for $T = 50$ ms with respect to the reference configuration, keeping the DM in the FM configuration. Using Table II, we expect a variation of $-1626(99)$ μGal of gravity due to the effect of the window aberrations. We attribute the difference between the calculated and measured values to the DM nonlinearities, which are significant for high deformations ($> 0.3\lambda$). Third, we repeat the gravity measurements for different values of T, represented by the blue triangles, in the presence of the additional window keeping the DM in the FM configuration.

Finally, the DM is shaped according to the corrections described earlier, and we recover the initial contrast of 17% at $T = 50$ ms, which we take as evidence of the efficiency

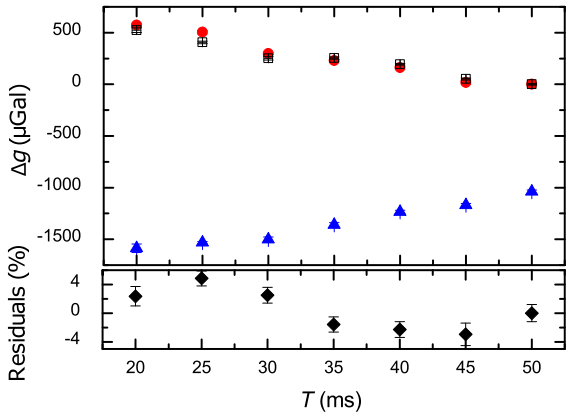

FIG. 6. Gravity measurements for different interferometer times $2T$ with and without an additional window, with and without an aberration correction. (Top) Open black squares represent the measurements realized with the DM in the flat map configuration before inserting the additional window. Blue triangles, after inserting the window. Red circles display the measurements realized with the aberrations compensated by the DM. (Bottom) Relative residuals after the compensation.

of the wavefront correction. This is confirmed by a last series of differential measurements, displayed as red circles. We find a good agreement with the initial measurements performed without the additional window, which demonstrates the efficiency of the compensation. Relative residuals (displayed as black diamonds at the bottom in Fig. 6) lie in between $\pm 4\%$. These differences can be explained by residual imperfections of the correction and fluctuations of the two-photon light shift.

VI. CONCLUSION

In conclusion, we demonstrate that the use of an appropriate deformable mirror allows one to correct the wavefront aberrations in atomic interferometers. Though the compensation is demonstrated here for the large distortions induced by an additional window of poor optical quality, it should also be effective for weaker aberrations thanks to the high resolution of the actuation and the excellent stability of the mirror. This could be demonstrated in state-of-the-art atom gravimeters, such as those of Refs. [2,4,13].

In addition, the large dynamical range of the DM and its short response time enable one, at the same time, to suppress Coriolis acceleration (compensating Earth's rotation by counterrotating the mirror during the interferometer sequence [40]) and reject ground vibration noise (by translating the mirror surface in real time [41] or right before the last Raman pulse, similar to Ref. [42]). These compensation techniques can be extended to other instruments based on atom interferometry, such as gravity gradiometers and gyroscopes. In particular, they would be relevant for large-scale experiments, such as based on large-momentum transfer beam splitters and/or long interferometer times. Indeed, in these experiments, the effect of wavefront aberrations scales as the effective momentum $n\hbar k$ imparted to the atoms, and the effect of high-order aberrations onto the inertial measurement increases with the interferometer duration $2T$.

ACKNOWLEDGMENTS

This work is supported by CNES (R&T R-S11/SU-0001-030). M. L. thanks Muquans for financial support. The authors thank Boston Micromachines Corporation for their assistance, A. Landragin for fruitful discussions, and E. Cocher, C. Janvier, H. Bouchiba, and M. Mazet for their contributions in the early stage of the experiment.

[1] A. D. Cronin, J. Schmiedmayer, and D. E. Pritchard, Optics and interferometry with atoms and molecules, Rev. Mod. Phys. **81**, 1051 (2009).

[2] Z.-K. Hu, B.-L. Sun, X.-C. Duan, M.-K. Zhou, L.-L. Chen, S. Zhan, Q.-Z. Zhang, and J. Luo, Demonstration of an ultrahigh-sensitivity atom-interferometry absolute gravimeter, Phys. Rev. A **88**, 043610 (2013).

[3] P. Gillot, O. Francis, A. Landragin, F. Pereira Dos Santos, and S. Merlet, Stability comparison of two absolute gravimeters: Optical versus atomic interferometers, Metrologia **51**, L15 (2014).

[4] C. Freier, M. Hauth, V. Schkolnik, B. Leykauf, M. Schilling, H. Wziontek, H.-G. Scherneck, J. Müller, and A. Peters, Mobile quantum gravity sensor with unprecedented stability, J. Phys. Conf. Ser. **723**, 012050 (2016).

[5] J. M. McGuirk, G. T. Foster, J. B. Fixler, M. J. Snadden, and M. A. Kasevich, Sensitive absolute-gravity gradiometry using atom interferometry, Phys. Rev. A **65**, 033608 (2002).

[6] F. Sorrentino, Q. Bodart, L. Cacciapuoti, Y. H. Lien, M. Prevedelli, G. Rosi, L. Salvi, and G. M. Tino, Sensitivity limits of a Raman atom interferometer as a gravity gradiometer, Phys. Rev. A **89**, 023607 (2014).

[7] T. L. Gustavson, A. Landragin, and M. A. Kasevich, Rotation sensing with a dual atom-interferometer sagnac gyroscope, Classical Quantum Gravity **17**, 2385 (2000).

[8] I. Dutta, D. Savoie, B. Fang, B. Venon, C. L. Garrido Alzar, R. Geiger, and A. Landragin, Continuous Cold-Atom Inertial Sensor with 1 nrad/sec Rotation Stability, Phys. Rev. Lett. **116**, 183003 (2016).

[9] J. B. Fixler, G. T. Foster, J. M. McGuirk, and M. A. Kasevich, Atom interferometer measurement of the Newtonian constant of gravity, Science **315**, 74 (2007).

[10] G. Rosi, F. Sorrentino, L. Cacciapuoti, M. Prevedelli, and G. M. Tino, Precision measurement of the newtonian gravitational constant using cold atoms, Nature (London) **510**, 518 (2014).

[11] R. Bouchendira, P. Cladé, S. Guellati-Khélifa, F. Nez, and F. Biraben, New Determination of the Fine Structure Constant and Test of the Quantum Electrodynamics, Phys. Rev. Lett. **106**, 080801 (2011).

[12] Ch. J. Bordé, Atomic interferometry with internal state labelling, Phys. Lett. A **140**, 10 (1989).
[13] A. Louchet-Chauvet, T. Farah, Q. Bodart, A. Clairon, A. Landragin, S. Merlet, and F. Pereira Dos Santos, The influence of transverse motion within an atomic gravimeter, New J. Phys. **13**, 065025 (2011).
[14] V. Schkolnik, B. Leykauf, M. Hauth, C. Freier, and A. Peters, The effect of wavefront aberrations in atom interferometry, Appl. Phys. B **120**, 311 (2015).
[15] M.-K. Zhou, Q. Luo, L.-L. Chen, X.-C. Duan, and Z.-K. Hu, Observing the effect of wave-front aberrations in an atom interferometer by modulating the diameter of raman beams, Phys. Rev. A **93**, 043610 (2016).
[16] A. Gauguet, B. Canuel, T. Lévèque, W. Chaibi, and A. Landragin, Characterization and limits of a cold-atom sagnac interferometer, Phys. Rev. A **80**, 063604 (2009).
[17] G. Tackmann, P. Berg, S. Abend, C. Schubert, W. Ertmer, and E. M. Rasel, Large-area sagnac atom interferometer with robust phase read out, C.R. Phys. **15**, 884 (2014).
[18] T. Kovachy, P. Asenbaum, C. Overstreet, C. A. Donnelly, S. M. Dickerson, A. Sugarbaker, J. M. Hogan, and M. A. Kasevich, Quantum superposition at the half-metre scale, Nature (London) **528**, 530 (2015).
[19] B. Altschul, Q. G. Bailey, L. Blanchet, K. Bongs, P. Bouyer, L. Cacciapuoti, S. Capozziello, N. Gaaloul, D. Giulini, J. Hartwig, L. Iess, P. Jetzer, A. Landragin, E. Rasel, S. Reynaud, S. Schiller, C. Schubert, F. Sorrentino, U. Sterr, J. D. Tasson, G. M. Tino, P. Tuckey, and P. Wolf, Quantum tests of the einstein equivalence principle with the ste-quest space mission, Adv. Space Res. **55**, 501 (2015).
[20] P. Hamilton, M. Jaffe, J. M. Brown, L. Maisenbacher, B. Estey, and H. Müller, Atom Interferometry in an Optical Cavity, Phys. Rev. Lett. **114**, 100405 (2015).
[21] I. Riou, N. Mielec, G. Lefèvre, M. Prevedelli, A. Landragin, P. Bouyer, A. Bertoldi, R. Geiger, and B. Canuel, A marginally stable optical resonator for enhanced atom interferometry, arXiv:1701.01473.
[22] H. W. Babcock, The possibility of compensating astronomical seeing, Publ. Astron. Soc. Pac. **65**, 229 (1953).
[23] F. Merkle, P. Kern, P. Léna, F. Rigaut, J. C. Fontanella, G. Rousset, C. Boyer, J. P. Gaffard, and P. Jagourel, Successful tests of adaptive optics, Messenger **58**, 1 (1989).
[24] S. Bonora, Distributed actuators deformable mirror for adaptive optics, Opt. Commun. **284**, 3467 (2011).
[25] D. A. Horsley, H. Park, S. P. Laut, and J. S. Werner, Characterization of a bimorph deformable mirror using stroboscopic phase-shifting interferometry, Sens. Actuators A **134**, 221 (2007).
[26] O. Cugat, S. Basrour, C. Divoux, P. Mounaix, and G. Reyne, Deformable magnetic mirror for adaptive optics: technological aspects, Sens. Actuators A **89**, 1 (2001).
[27] L. A. Poyneer, B. Bauman, B. A. Macintosh, D. Dillon, and S. Severson, Experimental demonstration of phase correction with a 32×32 microelectromechanical systems mirror and a spatially filtered wavefront sensor, Opt. Lett. **31**, 293 (2006).
[28] M. Kasprzack, B. Canuel, F. Cavalier, R. Day, E. Genin, J. Marque, D. Sentenac, and G. Vajente, Performance of a thermally deformable mirror for correction of low-order aberrations in laser beams, Appl. Opt. **52**, 2909 (2013).
[29] P. T. Beyersdorf, S. Zappe, M. M. Fejer, and M. Burkhardt, Cavity with a deformable mirror for tailoring the shape of the eigenmode, Appl. Opt. **45**, 6723 (2006).
[30] M. G. Tarallo, J. Miller, J. Agresti, E. D'Ambrosio, R. DeSalvo, D. Forest, B. Lagrange, J. M. Mackowsky, C. Michel, J. L. Montorio, N. Morgado, L. Pinard, A. Remilleux, B. Simoni, and P. Willems, Generation of a flat-top laser beam for gravitational wave detectors by means of a nonspherical Fabry-Perot resonator, Appl. Opt. **46**, 6648 (2007).
[31] J. Le Gouët, T. E. Mehlstäubler, J. Kim, S. Merlet, A. Clairon, A. Landragin, and F. Pereira Dos Santos, Limits to the sensitivity of a low noise compact atomic gravimeter, Appl. Phys. B **92**, 133 (2008).
[32] S. Merlet, L. Volodimer, M. Lours, and F. Pereira Dos Santos, A simple laser system for atom interferometry, Appl. Phys. B **117**, 749 (2014).
[33] M. Kasevich and S. Chu, Atomic Interferometry Using Stimulated Raman Transitions, Phys. Rev. Lett. **67**, 181 (1991).
[34] J. Y. Wang and D. E. Silva, Wave-front interpretation with Zernike polynomials, Appl. Opt. **19**, 1510 (1980).
[35] B. C. Platt and R. Shack, History and principles of Shack-Hartmann wavefront sensing, J. Refract. Surg. **17**, S573 (2001).
[36] K. M. Morzinski, J. W. Evans, S. Severson, B. Macintosh, D. Dillon, D. Gavel, C. Max, and D. Palmer, Characterizing the potential of mems deformable mirrors for astronomical adaptive optics, Proc. SPIE Int. Soc. Opt. Eng. **6272**, 627221 (2006).
[37] T. Farah, P. Gillot, B. Cheng, A. Landragin, S. Merlet, and F. Pereira Dos Santos, Effective velocity distribution in an atom gravimeter: Effect of the convolution with the response of the detection, Phys. Rev. A **90**, 023606 (2014).
[38] S. M. Dickerson, J. M. Hogan, A. Sugarbaker, D. M. S. Johnson, and M. A. Kasevich, Multiaxis Inertial Sensing with Long-Time Point Source Atom Interferometry, Phys. Rev. Lett. **111**, 083001 (2013).
[39] A. Gauguet, T. E. Mehlstäubler, T. Lévèque, J. Le Gouët, W. Chaibi, B. Canuel, A. Clairon, F. Pereira Dos Santos, and A. Landragin, Off-resonant Raman transition impact in an atom interferometer, Phys. Rev. A **78**, 043615 (2008).
[40] S.-Y. Lan, P.-C. Kuan, B. Estey, P. Haslinger, and H. Müller, Influence of the Coriolis Force in Atom Interferometry, Phys. Rev. Lett. **108**, 090402 (2012).
[41] J. M. Hensley, A. Peters, and S. Chu, Active low frequency vertical vibration isolation, Rev. Sci. Instrum. **70**, 2735 (1999).
[42] J. Lautier, L. Volodimer, T. Hardin, S. Merlet, M. Lours, F. Pereira Dos Santos, and A. Landragin, Hybridizing matter-wave and classical accelerometers, Appl. Phys. Lett. **105**, 144102 (2014).